Supporting Information

Structural control of fibrin bioactivity by mechanical deformation

Sachin Kumar[1,2,3]*, Yujen Wang[1], Mohammadhasan Hedayati[1], Frederik Fleissner[4], Manuel K. Rausch[1,5,6], and Sapun H. Parekh[1,4,*]

[1] Department of Biomedical Engineering, University of Texas at Austin, 107 W. Dean Keeton Rd., Austin, TX 78712, USA

[2] Centre for Biomedical Engineering, Indian Institute of Technology Delhi, Hauz Khas, New Delhi, 110016, India

[3] Department of Biomedical Engineering, All India Institute of Medical Sciences, New Delhi, 110029, India

[4] Molecular Spectroscopy Department, Max Planck Institute for Polymer Research, Ackermannweg 10, Mainz 55128, DE

[5] Oden Institute for Computational Engineering and Sciences, University of Texas at Austin, 201 E 24th St, Austin, TX 78712

[6] Department of Aerospace Engineering & Engineering Mechanics, University of Texas at Austin, 2617 Wichita St, Austin, TX 78712

* corresponding authors: sachin.kumar@cbme.iitd.ac.in, sparekh@utexas.edu

This supporting information file includes

Materials and Methods

Supporting Figures and data

Movie S4: Z-stack confocal images of 100% strained fibrin showing distribution of ThT and tPA. 45 μm depth, 3 μm slice spacing, 112 μm x 112 μm image size

Movie S5: Z-stack confocal images of unbinding of tPA upon mechanical straining of fibrin. 50 μm depth, 5 μm slice spacing, 112 μm x 112 μm image size

Materials and Methods

Preparation of fibrin hydrogel substrate,

Figure S1 shows the preparation process of fibrin hydrogels in our experiments. Briefly, a thick (1 mm) PDMS sheet (Gel-Pak) was cut into a rectangular mold and placed on a supporting thin PDMS sheet (100 μm thickness) (Gel-Pak) lying on a glass slide. The assembly was treated with ultraviolet ozone (UVO) for 30 min to render hydrophilic surfaces. UVO has been shown to increase surface wettability and adhesion properties of PDMS for protein adsorption (1) (2) and improve fibrin adhere to the thin PDMS sheets. To make each fibrin hydrogel, a fresh fibrin(ogen) solution: 7.5 mg/ml fibrinogen (FIB 2, Enzyme Research Laboratories) in FB1X buffer (20 mM HEPES, 5 mM $CaCl_2$ and 150 mM NaCl (all from Sigma) at pH 7.4) was prepared. Thrombin (Factor IIa, Enzyme Research Laboratories) at a final concentration of 1.0 U/ml was mixed with the fibrinogen solution, and the solution was immediately pipetted into the rectangular mold. The solution was covered with another (non-UVO treated) thin PDMS sheet in a direct contact with the solution and a coverslip. The sandwiched fibrinogen solution was allowed to polymerize for 2 hr at 37 °C and 95% relative humidity. After polymerization, the top (covering) thin PDMS sheet, coverslip, and rectangular PDMS mold were carefully and slowly removed to obtain an intact fibrin hydrogel on the supporting PDMS sheet.

Tensile deformation of fibrin gels

For tensile deformation of fibrin networks, the thin supporting (100 μm thickness) PDMS sheet, upon which the polymerized fibrin gel adhered, was stretched with a motorized tensile stretcher to 100% of its initial length, which resulted in 73% strain of the fibrin gel at the free surface. **Movie S1 and Supporting Figure S2(A) and (D)** show the stretching process and images of unstrained and strained samples, and transmission of strain to fibrin gel through PDMS sheet. The stretched fibrin gels were clamped using in-house clamps as shown in **Figure S2(B)** to hold the strain on the PDMS sheet for further studies and characterization. All studies and characterization on the stretched fibrin samples were performed as soon as possible, and the samples were kept fully hydrated in FB1X for the duration of experiments.

Characterization of fibrin morphology

Fibrin morphology was imaged using reflectance with an upright laser scanning confocal microscope (LSM-510, Zeiss) and a 40X, 1.0 NA water-dipping objective (Zeiss). Fibrin networks were illuminated with a 488 nm laser and reflected light was collected by setting the Meta detector channel between 475-500 nm wavelength in accordance to previous literature (3). The diameter of fibrin fibers was measured on raw images using ImageJ. In addition, AC mode atomic force microscopy (AFM, Dimension Icon, Bruker) with AC160TS-R3 cantilevers were used to image fibrin sample morphology of (dried) unstrained and strained conditions.

Molecular characterization of fibrin

Changes in fibrin molecular structure upon mechanical deformation were evaluated using attenuated total internal reflection infrared (ATR-IR) spectroscopy measurements. For these experiments, unstrained and tensile strained fibrin hydrogel networks were mounted on custom-built hollow Teflon molds (shown in **Figure S2(C)**) and placed over the ATR crystal surface to achieve good contact. ATR-IR spectra were collected using a TENSOR II Bruker spectrometer equipped with a DGTS detector. Typically, for each spectrum, 128 interferograms were collected and averaged in single-beam mode at a resolution of 4 cm^{-1}. Spectra from three different spots on each sample were averaged for analysis. For structural analysis, decomposition of the ATR-IR spectra of the Amide I and II regions using OriginPro was done by setting component peak locations found by second-derivative analysis (**Figure S3**) in accordance to previously reported literature (4). Lorentzian profiles were used to fit the envelope of the amide band spectra. The peak widths and their positions were assigned to respective secondary structure in accordance with previous work on fibrin (4, 5) (detailed information is provided in the Supporting Information). Peak areas were calculated from the fits in OriginPro to quantify the fraction of respective secondary structures in protein.

Molecular microscopy of single fibrin fibers

In addition to bulk spectroscopy, we used stimulated Raman scattering (SRS) spectro-microscopy (SRS) to image fibrin molecular structure *in situ*. A fibrinogen solution, containing 0.2 mg/ml of fibrinogen and 1U/ml of thrombin in FB1X was spread across two sheets of pre-hydrated lens paper glued to glass cover slips. The coverslips were affixed between the jaws of a vernier caliper with a ~ 1 mm gap as schematically showed in **Figure S4(A)**. The entire caliper assembly was placed into an oven at 37 °C for 2 hr with 95% RH. After polymerization, two pieces

of standard colored lab tape (Fisher) were placed on top of the lens paper, but not directly on the sample, to hold water across the caliper gap. Thereafter, jaws of the caliper were widened such that the fibrin fibers spanning the gap were stretched by a nominal strain of ~ 100% as shown in **Figure S4(B)**.

SRS spectral images of unstrained and strained fibrin were acquired using a femtosecond laser with two outputs (Insight X3 Dual, Spectra-Physics) with a fixed 1045 nm beam (used as the Stokes) and a tunable beam from 680 to 1300 nm (used as the pump). The repetition rate of the laser was 80 MHz. The two laser beams were spatially and temporally overlapped using a spectral focusing and timing recombination unit (SF-TRU, Newport), and the 1045 nm beam was modulated with an electro-optic modulator at 19.7 MHz in the SF-TRU (6). The output laser from the SF-TRU were chirped to ~ 7 ps for spectral focusing. The beams were overlapped and were routed to the sample via the laser scanner of a confocal microscope (FV3000, Olympus) using with standard protected silver mirrors and periscope (Newport). A 20X, 0.4 NA air objective (Olympus) was used to focus the lasers into the samples. SRS signals were collected in the transmitted direction using a 40X, 1.0 NA dipping objective (Zeiss). SRS was detected as modulation (loss) of the pump laser after filtering the Stokes beam with a short pass 950 nm filter (FESH0950, Thorlabs) and imaging the back focal plane of the objective onto a lock-in detector (SRS Detection Module, APE) with a 75 mm and 60 mm Keplerian telescope after the collection objective.

SRS images (512 x 512 pixels) and spectra in the CH stretch region were collected with the pump tuned to 802 nm with a dwell time of 2 μs per pixel with a total power of 100 mW sent into the scanner. A spectral stack of images with 200 frames was collected from 2850 – 3050 cm^{-1} with spectral resolution of ~4 cm^{-1} by changing the delay between the two beams with a motorized stage that was synchronized with the microscope frame acquisition. SRS images in the Amide I region for the α-helix and β-sheet modes were acquired by tuning the pump laser to 890 nm and scanning the delay between the two beams to tune the vibrational modes. We used 1650 cm^{-1} for the α-helix mode and 1670 cm^{-1} for the β-sheet mode. In this case, we used a combined power of 150 mW going on the scanner. The delay-wavenumber calibration of the SF-TRU for the CH and Amide regions was done with polystyrene with identical tuning wavelength, chirp parameters, and delay ranges.

Image J was used to quantify Amide I spectral images via thresholding to calculate total segmented area for helix (1650 cm^{-1}) and β-sheet (1670 cm^{-1}) respectively (detailed images are provided in the Supporting Information **Figure S5**). The ratio of segmented area of α-helix to β-sheet was expressed as area fractional value of helix:sheet.

Reversibility of strain-induced structural changes in fibrin gels

Reversibility of mechanical deformation induced secondary structural changes in fibrin gels was studied using CARS microspectroscopy in accordance with our previous work (7). The details of CARS microspectroscopy setup and CARS data processing have been extensively described in our previous research work (7). Strained gels were allowed to relax for 20 minutes before CARS imaging.

Imaging biochemical activity and molecular structure on bulk fibrin gels

Thioflavin T (ThT, Sigma) and tissue plasminogen activator (tPA) with a FITC label (tPA-FTIC, Abcam) were used to probe the molecular structure and biochemistry of bulk fibrin gel (7.5 mg/ml) respectively. ThT solution (100 μM) was prepared as specified by the supplier and incubated with fibrin hydrogel networks (both unstrained and strained) for 30 min. After five washes with phosphate-buffered saline (PBS), bound ThT fluorescence was imaged by exciting at 450 nm and collecting emission from 480-530 nm. Similarly, fibrin networks (unstrained and strained) were incubated with a tPA-FITC (20 μM) protein solution for 30 min, washed with PBS five times and imaged in fluorescence by exciting at 488 nm and collecting emission from 530-580 nm. All images were collected with LSM-510 confocal microscope on gels prepared on PDMS sheets.

Cyclic straining of fibrin and ThT binding was studied using a home-built deformation stage as described in our previous study (8). Independent fibrin networks were used for each strain condition as follows. Unstrained bulk fibrin networks on the deformation stage were strained with ThT and imaged using FV-3000 confocal microscope (cycle1-0%). An independent fibrin network was deformed on the deformation stage to 80% strain, stained with ThT, and imaged (cycle1-80%). Another fibrin gel was strained, allowed to sit for 20 minutes, and the strain was released to 0% after which the gel was stained with ThT and imaged (cycle2-0%). Finally, another fibrin gel was strained to 80%, relaxed, and strained again to 80% before staining with ThT. All images were

taken with 488 nm excitation. For the quantification, all images were taken with identical acquisition settings. The images often saturated in the strained case, but the gain settings and laser power used were necessary to visualize any ThT fluorescence in the unstrained fibrin gels. Average fluorescence intensity was measured from a set of three of samples for each condition.

Imaging biochemical activity and molecular structure on single fibrin fibers

We also evaluated binding of tPA and ThT to single unstrained and strained fibrin fibers. For these experiments, a 0.2 mg/ml fibrinogen solution with 1 U/ml thrombin (in FB1X) was prepared on across a supporting thin PDMS films each attached to thick PDMS blocks on each side of a vernier caliper as shown in **Figure S7(A-C)**. Sparse fibrin networks were incubated with tissue plasminogen activator (tPA) with either Texas Red tPA (Abcam) or ThT to and washed as described previously. Some experiments used 10% molar ratio of Alexa 488-labeled (Life Technologies) fibrinogen as indicated.

Stretching was done the microscope stage with the caliper, such that samples could be imaged directly with the FV-3000 confocal microscope. The caliper jaws holding the PDMS blocks were stretched apart by 100% of their initial separation (**Figure S7(C)**). All confocal images were captured under identical operating conditions using 20X, 0.4 NA air objective (Olympus).

Platelet isolation and measurement of attachment and morphology on fibrin hydrogels

Blood from a de-identified, healthy volunteer was drawn into acid citrate dextrose (ACD) and EDTA vacutainer tubes by a licensed physician in accordance with the standard protocol approved by the institute with informed consent. Platelets were isolated from whole blood by differential centrifugation in accordance with the previously established methods (9). In brief, the whole blood was centrifuged at 800 rpm for 10 min to obtain platelet rich plasma (PRP). PRP was then centrifuged at 1500 rpm for 5 min to obtain a platelet pellet. The platelet pellet was suspended and diluted to final density of 10^5 /ml in HEPES Tyrode's buffer (pH 7.4) supplemented with 0.1% BSA. The morphology of the obtained platelets was verified by brightfield microscopy (IX-81, Olympus) with a 40X, 0.75 NA objective (Olympus).

Obtained platelets were immediately labeled with 1μM Calcein green AM dye for 15 min at room temperature and seeded on unstrained or strained fibrin hydrogels as previously reported (10). The platelet-fibrin mixture was incubated for 2 hr at 37°C in CO_2 incubator. After incubation,

samples were washed several times with HEPES Tyrode's buffer to remove non-adhered platelets. The remaining adhered platelets were fixed with 4% formaldehyde solution. Platelet attachment and morphology were quantified using fluorescence microscopy with the LSM-510 confocal laser scanning microscope and scanning electron microscopy (SEM, LEO Gemini 1530, Germany). All platelet experiments were performed within 5 hr of the whole blood collection to avoid cell death and intrinsic activation.

Binding assay of platelet integrins to fibrin

Platelet integrin ($\alpha_{IIb}\beta_3$) binding activity to fibrin was using microspheres as substrates for the extracellular domain of $\alpha_{IIb}\beta_3$ integrin. Recombinant human $\alpha_{IIb}\beta_3$ integrin (Abcam) (1 mg/ml) was mixed with fluorescent microspheres (Fluoresbrite-Carboxylate, 1.75µm diameter) suspended in PBS (10^8 beads/ml). The solution was then placed on a shaker at 300 rpm for 24 hr at 4°C for adsorption of integrins on the surface of beads. Beads were collected by centrifugation (10000 rpm for 5 min) and washed twice with PBS to remove unbounded integrin. Thereafter, integrin-coated beads were blocked with 2 % BSA-FITC (Sigma) solution for 24 hr at 4°C. For control experiments, BSA-coated beads were prepared in accordance to above mentioned protocol without any integrin coating. Finally, integrin-coated (or BSA-coated) beads were pelleted, washed twice, and re-suspended in PBS (10^7 beads/ml) containing 1 mM $MnCl_2$ (or just PBS for BSA-coated beads). SDS-PAGE was used for the characterization of bounded proteins (integrin $\alpha_{IIb}\beta_3$ and BSA) to the microbeads **(Figure S11)**.

For integrin binding assays, unstrained and strained fibrin hydrogels were incubated with integrin-coated (or BSA-coated) microbeads and allowed to bind for 1 hr at room temperature followed by multiple rinses with PBS to remove unbound beads. Rinsed fibrin samples were imaged using confocal laser scanning microscopy (LSM 510), and the area density of microspheres was quantified from multiple fields of view using ImageJ.

Statistical analysis

Significant differences between experimental groups were analyzed using 1-way ANOVA (analysis of variance) with Tukey's test for multiple comparisons using OriginPro. Differences were considered statistically significant for $p < 0.05$ and indicated by symbols in the figures.

Preparation process of fibrin hydrogels on thin PDMS sheets

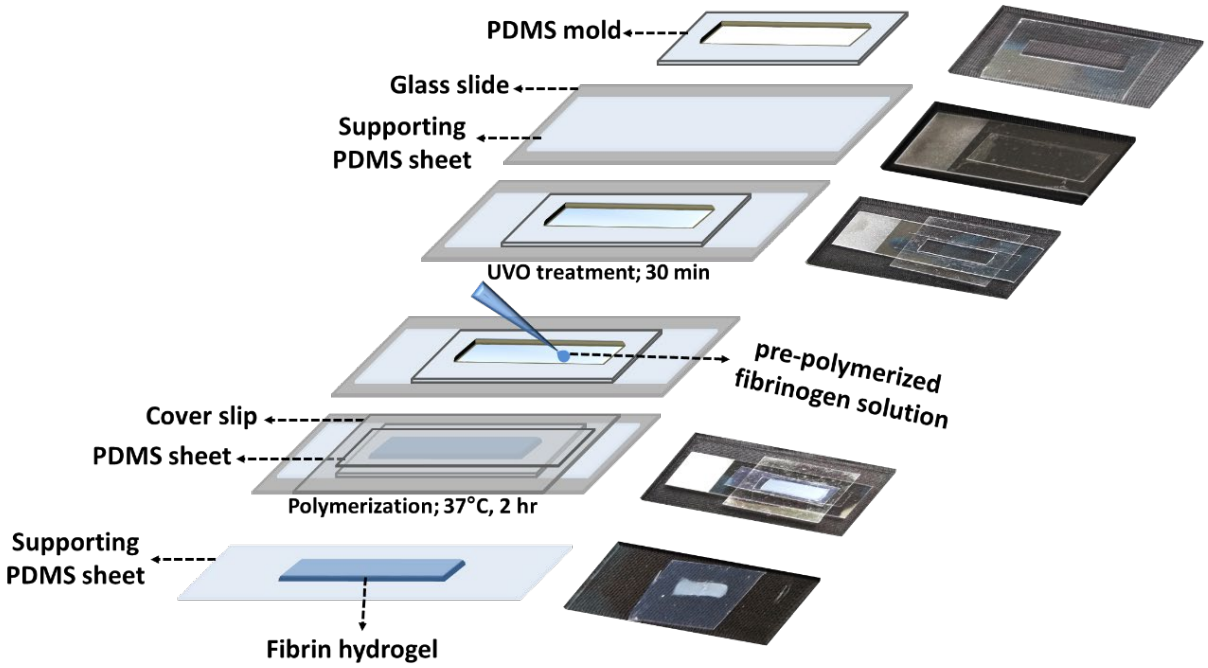

Figure S1: Schematic illustration of fibrin hydrogel on flexible PDMS sheets. Corresponding digital images show the process of sample preparation on flexible PDMS sheets.

Fibrin stretching on thin PDMS sheets and strain transmission from PDMS to fibrin network

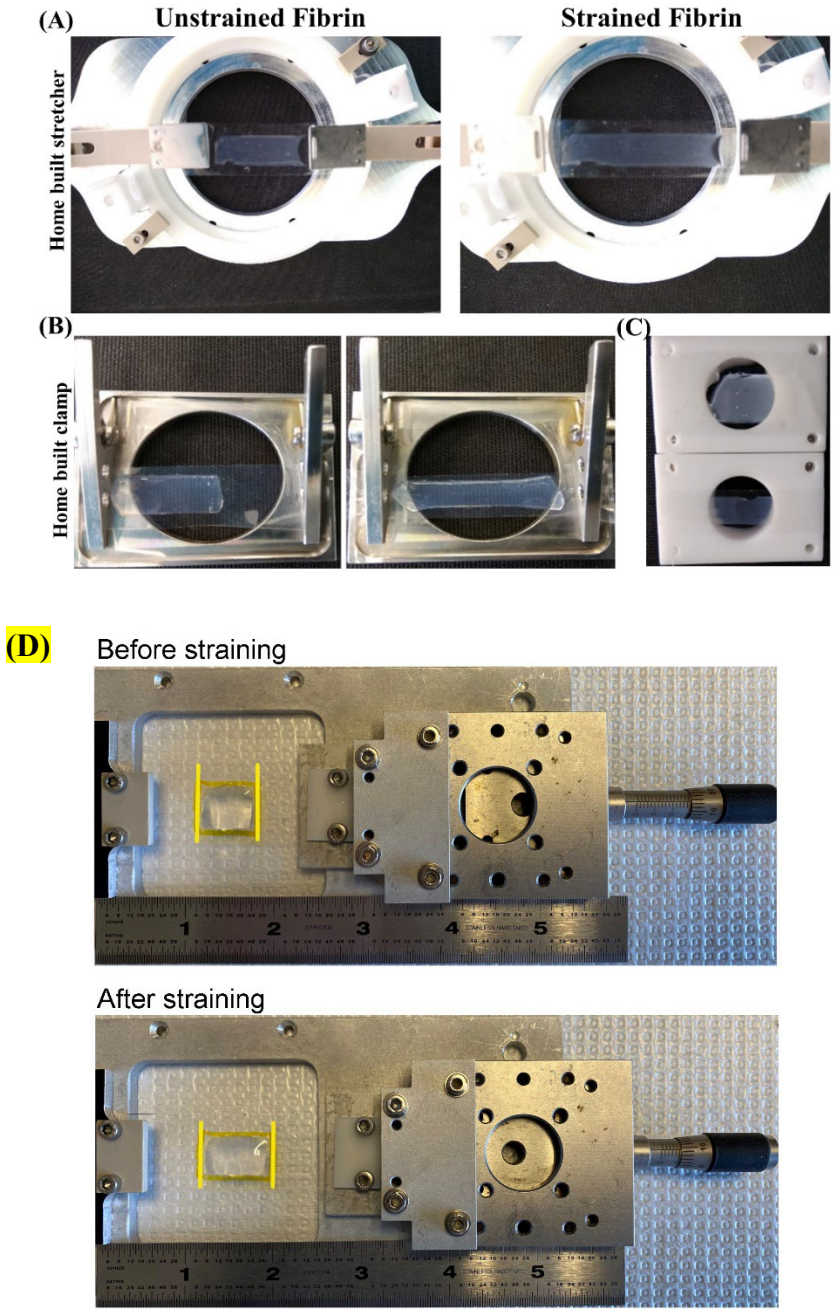

Figure S2: Fibrin stretching on thin PDMS sheets and strain transmission from PDMS to fibrin network. (A) Digital images of initial unstrained and 100% strained fibrin using home-built mechanical stretcher, (B) and (C) Clamping of unstrained and stained fibrin gel using home-built clamps. (D) Measurement of strain transfer from the PDMS sheet to the free surface of the fibrin gel after 100% strain was applied to the PDMS sheet.

Characterization of fibrin structure by ATR-IR spectroscopy

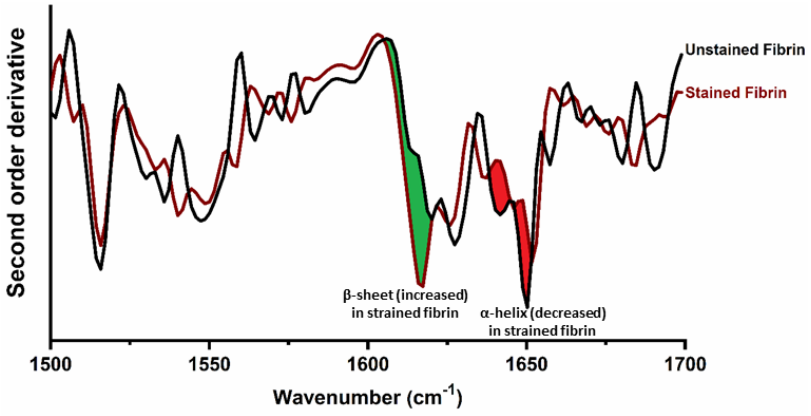

Figure S3: Second derivative of IR spectra of unstrained and 100% strained fibrin showing increase in β-sheet content (area highlighted in green) and decrease in α helix content (area highlighted in red) upon mechanical deformation.

Table S1: Fitting parameters for ATR-IR spectra of unstrained fibrin

Peak center (cm^{-1})	FWHM (cm^{-1})	Peak Area (%)	Peak assignment(4, 5, 11, 12)
1517	13	4.2	Random coil
1532	20	8.9	β-sheet
1550	32	19.7	α-helix
1616	21	9.6	β-sheet
1630	21	17.7	β-sheet
1644	21	19.1	Random coil
1655	21	14.4	α-helix
1673	20	6.4	turns/loops

Table S2: Fitting parameters for ATR-IR spectra of 100% unstrained fibrin

Peak center (cm^{-1})	FWHM (cm^{-1})	Area (%)	Peak assignment(4, 5, 11, 12)
1519	13	4.4	Random coil
1536	21	10.2	β-sheet
1554	32	17.7	α-helix

1618	29	26.0	β-sheet
1632	21	13.6	β-sheet
1645	18	12.1	Random coil
1655	16	8.6	α-helix
1667	14	5.0	turns/loops
1679	11	2.4	turns/loops

Preparation of single fibrin fibers and characterization of fibrin structure by SRS microscopy

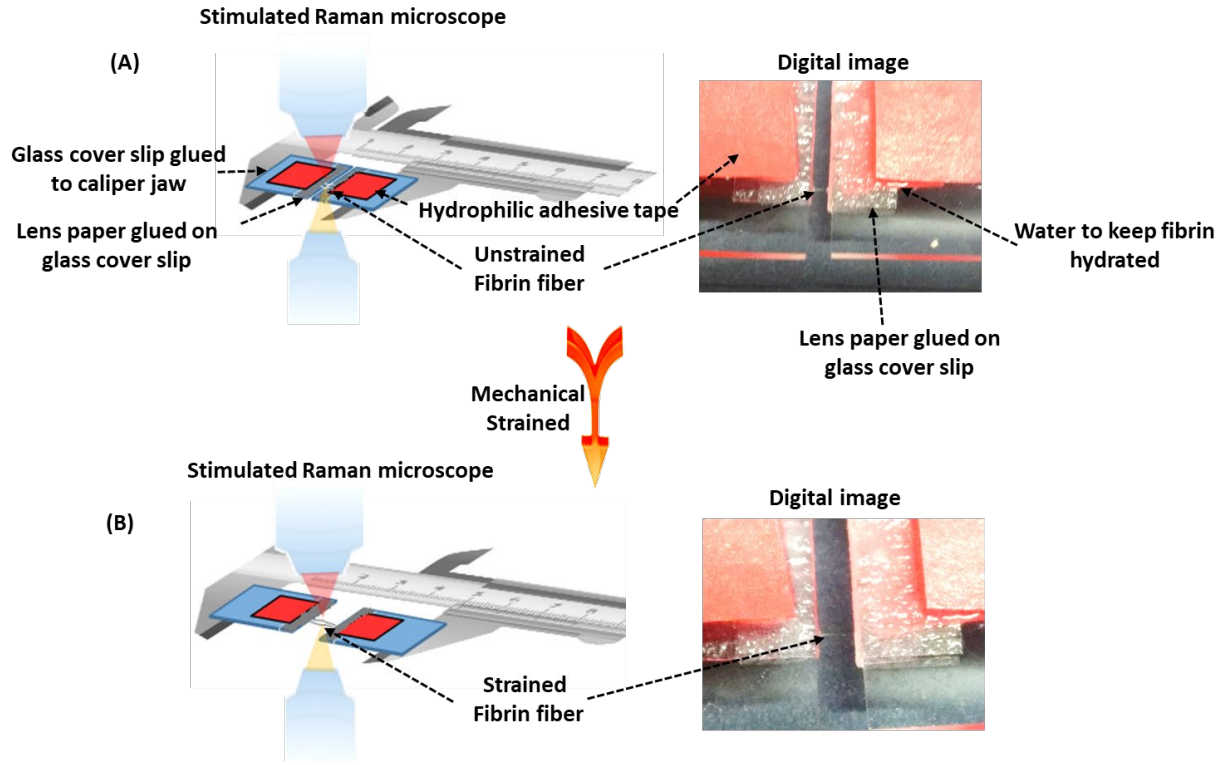

Figure S4: (A) and (B) illustration preparation of single fibrin preparation for SRS imaging. Digital images show single fibrin bundle on Vernier caliber setup. The caliper was used to apply strain.

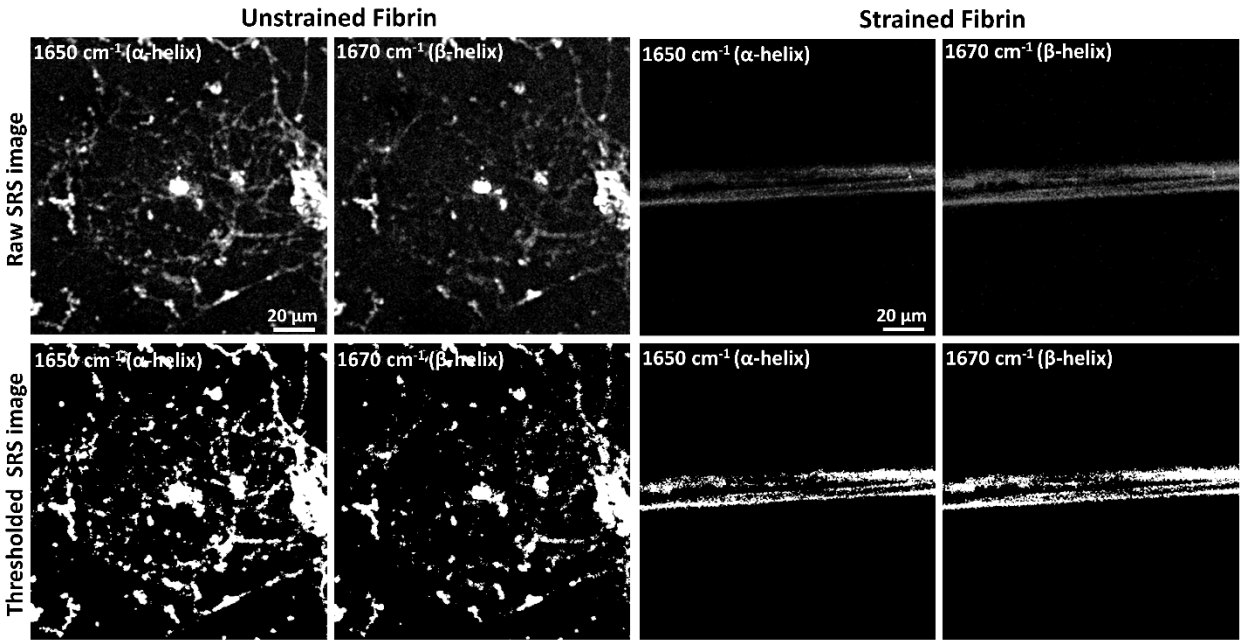

Figure S5: SRS spectral images of fibrin fibers before and after thresholding.

Reversibility of strain-induced secondary structural changes in fibrin

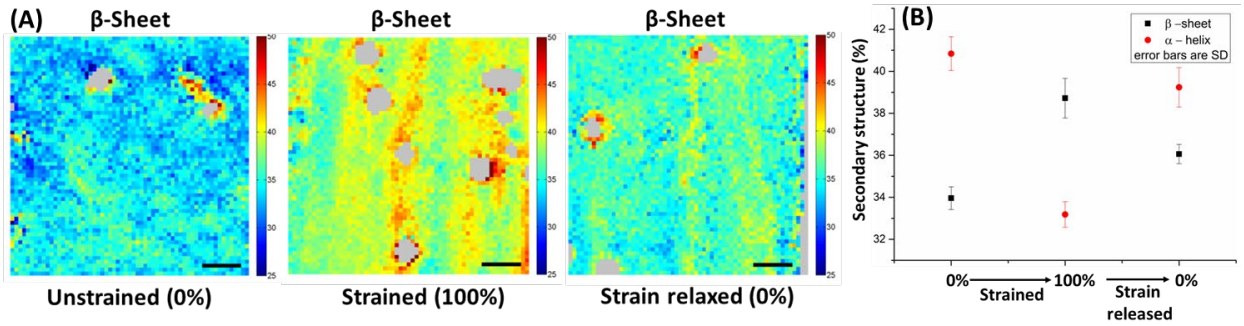

Figure S6: Structural reversibility in Fibrin hydrogel. (A) CARS Image and (B) secondary structure plot for unstained (0%), strained (100%), and strained released fibrin gel (scale bar = 5 µm). Error bars are from fitting amide modes of different pixels in the images.

Preparation of sparse fibrin networks to measure binding of biochemical dye (ThT) and (tPA)

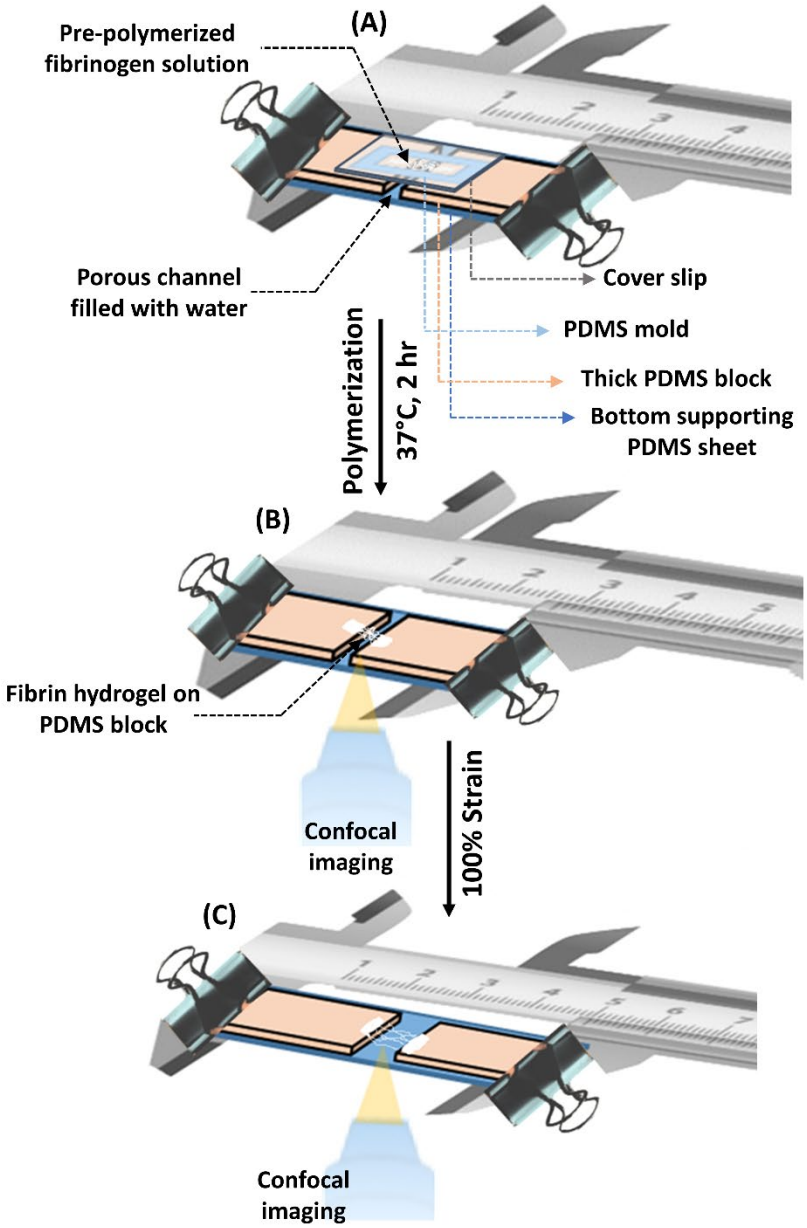

Figure S7: (A-C) Schematic illustration of preparation of sparse fibrin networks between two PDMS blocks for confocal imaging for bound tPA and ThT. The caliper was used to apply strain.

Differential binding and distribution of tPA and ThT to unstrained and strained bulk fibrin hydrogels

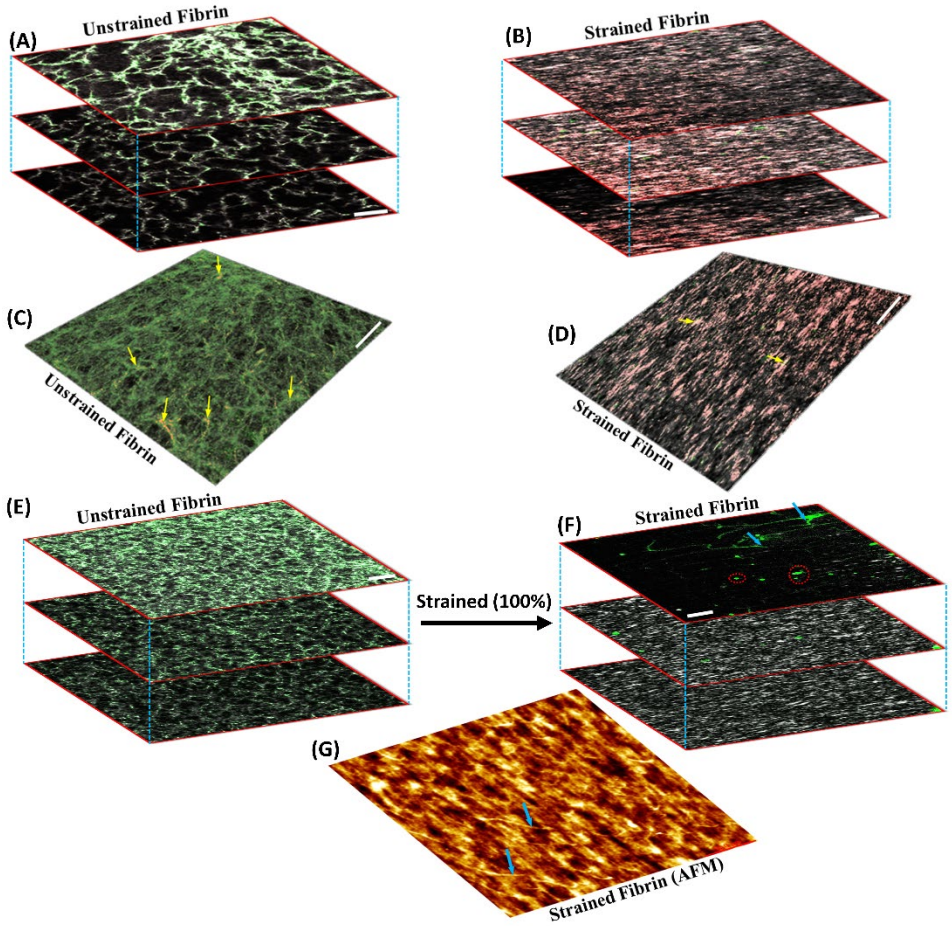

Figure S8: Differential binding and distribution of tPA and ThT to unstrained and strained bulk fibrin hydrogels (A) and (B). Images are from different sample depths (top to bottom: surface to 50 µm depth) profile of tPA (green) and ThT (red). (C) and (D) Maximum intensity projection images from Z-stacks (surface to 50 µm depth) of co-localization of tPA (green) and ThT (red) on unstrained and 100% strained bulk fibrin hydrogel networks, respectively. Yellow arrows show areas of ThT and tPA co-localization. (E) Images at different sample depths (top to bottom: surface to 50 µm depth) showing tPA binding (green) on unstrained bulk fibrin (grey), (F) images at different sample depths (top to bottom: surface to 50 µm depth) of the same bulk fibrin sample as in (E) shows unbinding of tPA upon 100% tensile deformation. Blue arrows and red circle show highlight broken fibers with tPA binding after straining fibrin. (G) AFM profile of tensile deformed fibrin sample. Arrows show broken fibers. Scale bar = 10 µm for optical images (A-F) and 5 µm for AFM image.

ThT binding on cyclically strained fibrin

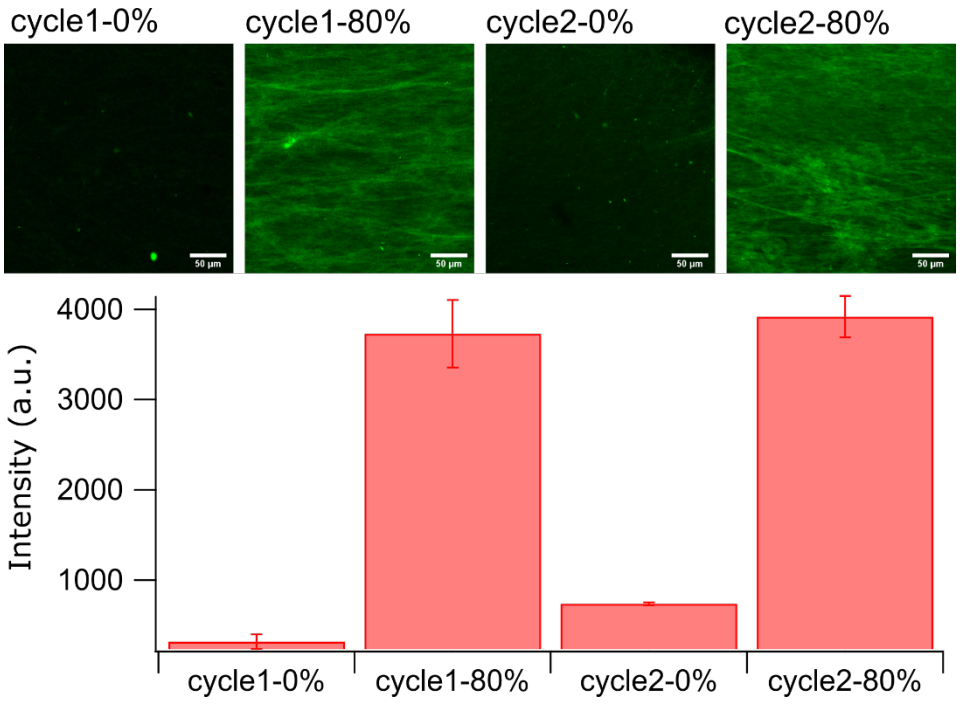

Figure S9: Reversible binding of ThT binding to bulk fibrin network under cyclic tensile loading. All images were taken with 488 nm excitation. For the quantification in the bar graph, all images were taken with identical acquisition settings to allow for comparison, and the mean intensity was taken from ImageJ. The images often saturated in the strained case, but the gain settings used were necessary to visualize any ThT fluorescence in the unstrained fibrin gels. The errors bars were calculated from the standard deviation of 3 fields of view from 3 different samples for each strain condition. For the representative images shown above the graph, the cycle1-0% strain and cycle2-0% strain images were taken from a high PMT gain to see structures while the cycle1-80% strain and cycle2-80% strain images were taken from a lower PMT gain so as to not saturate the detector.

Platelet isolation and binding to fibrin networks

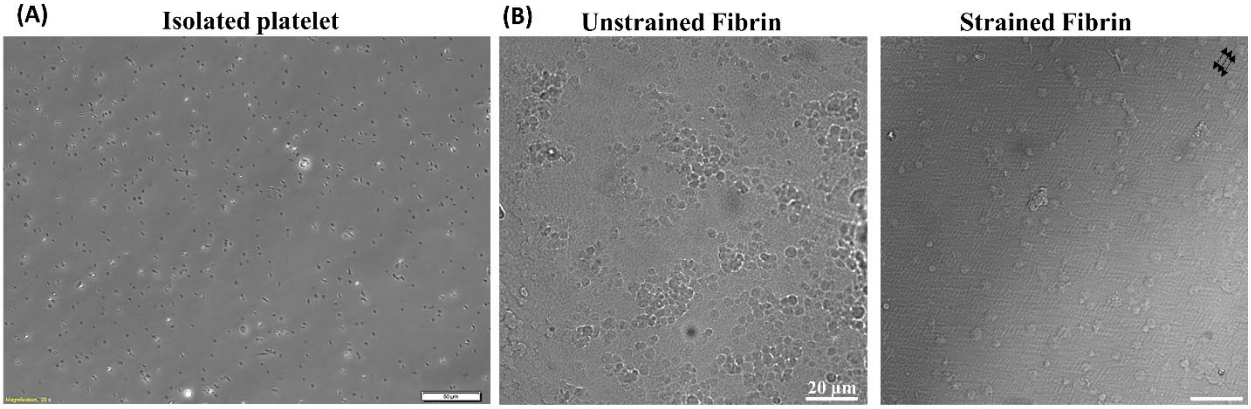

Figure S10: Platelet attachment upon exposure to differently strained fibrin. (A) Isolated platelet morphology from brightfield images show well-dispersed individual platelets without any aggregate morphology (scale bar = 50 µm). (B) Bright field images of attached platelets on unstrained and 100% strained fibrin (black arrows indicate direction of fibrin stretch).

Characterization of bound integrin proteins to the microbeads

Sodium dodecyl sulfate (SDS) polyacrylamide gel electrophoresis (PAGE) was employed to characterize bound protein (integrin and BSA) on microbeads. Proteins coated microbeads were loaded into sample buffer (NuPAGE LDS) on 4–12% gradient gels and run against standard integrin and BSA as control along with high-molecular-weight marker (ranging from 10 to 225 kDa (Novagen)) as described previously (13).

Figure S11 shows a Coomassie stained SDS PAGE gel of integrin and BSA proteins from coated microbeads. Integrin and BSA protein bands from beads were compared with unattached integrin and BSA as controls. Lane 1 with pristine beads alone showed no protein, as expected. . Lane 2 for commercial BSA-FITC showed presence of strong protein bands around 62 kDa, Lane 3 showed BSA from BSA-coated beads, which was similar to the BSA control band (Lane 2). Control integrin ($\alpha_{IIb}\beta_3$) in lane 4 showed presence of two bands round 100 kDa. As integrin ($\alpha_{IIb}\beta_3$) is composed of two different protein chain (α_{IIb}) and (β_3) which are linked by disulfide bond. Under reducing conditions for SDS PAGE, integrin ($\alpha_{IIb}\beta_3$) separates into two subunit bands at 125 kDa and 108 kDa for α_{IIb} and β_3, respectively (14, 15). Lane 5 shows beads coated with BSA-FITC, which is identical to Lanes 2 and 3. Similarly, in Lane 6, beads coated with BSA and integrin

showed presence of specific protein bands for BSA at 62 kDa and for integrin two subunits as shown by arrows.

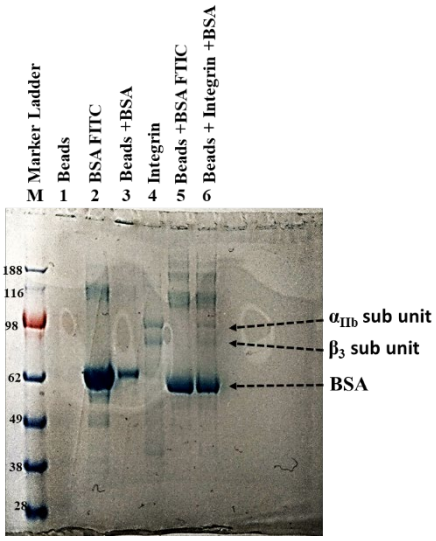

Figure S11: SDS page analysis of platelet integrin and BSA coated microbeads. Digital image of SDS PAGE gel of protein-coated beads that was used for platelet integrin experiments.

Binding of BSA-coated beads to fibrin hydrogels

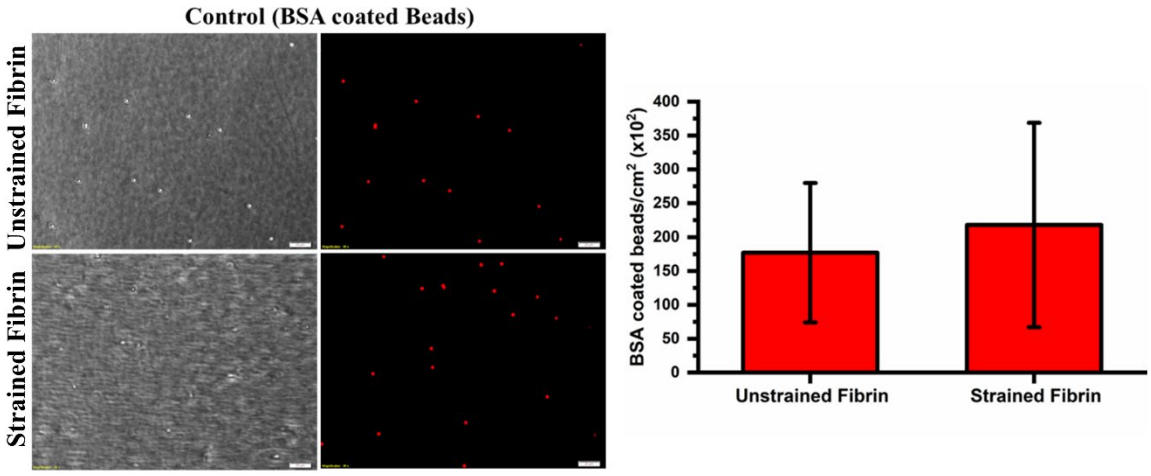

Figure S12: Fluorescence micrograph and quantification of bound BSA-coated micro-beads on unstrained and strained fibrin (Scale bar = 20 micron). There was no statistical difference.

References

1. Özçam AE, Efimenko K, & Genzer J (2014) Effect of ultraviolet/ozone treatment on the surface and bulk properties of poly (dimethyl siloxane) and poly (vinylmethyl siloxane) networks. *Polymer* 55(14):3107-3119.

2. Lin T-Y, Pfeiffer TT, & Lillehoj PB (2017) Stability of UV/ozone-treated thermoplastics under different storage conditions for microfluidic analytical devices. *RSC advances* 7(59):37374-37379.

3. Crosby CO*, et al.* (2019) Quantifying the Vasculogenic Potential of Induced Pluripotent Stem Cell-Derived Endothelial Progenitors in Collagen Hydrogels. *Tissue Engineering Part A* 25(9-10):746-758.

4. Litvinov RI, Faizullin DA, Zuev YF, & Weisel JW (2012) The α-helix to β-sheet transition in stretched and compressed hydrated fibrin clots. *Biophysical journal* 103(5):1020-1027.

5. Lindon JC, Tranter GE, & Koppenaal D (2016) *Encyclopedia of spectroscopy and spectrometry* (Academic Press).

6. Zeytunyan A, Baldacchini T, & Zadoyan R (2018) Module for multiphoton high-resolution hyperspectral imaging and spectroscopy. *Multiphoton Microscopy in the Biomedical Sciences XVIII*, (International Society for Optics and Photonics), p 104980K.

7. Fleissner F, Bonn M, & Parekh SH (2016) Microscale spatial heterogeneity of protein structural transitions in fibrin matrices. *Science advances* 2(7):e1501778.

8. Wang Y*, et al.* (2021) Probing fibrin's molecular response to shear and tensile deformation with coherent Raman microscopy. *Acta Biomaterialia* 121:383-392.

9. Lam WA*, et al.* (2011) Mechanics and contraction dynamics of single platelets and implications for clot stiffening. *Nature materials* 10(1):61-66.

10. Kim OV, Litvinov RI, Alber MS, & Weisel JW (2017) Quantitative structural mechanobiology of platelet-driven blood clot contraction. *Nature communications* 8(1):1-10.

11. Olsztynska-Janus S*, et al.* (2012) Spectroscopic techniques in the study of human tissues and their components. Part I: IR spectroscopy. *Acta of Bioengineering & Biomechanics* 14(3).

12. Olsztyńska-Janus S, Pietruszka A, Kiełbowicz Z, & Czarnecki M (2018) ATR-IR study of skin components: Lipids, proteins and water. Part I: Temperature effect. *Spectrochimica Acta Part A: Molecular and Biomolecular Spectroscopy* 188:37-49.

13. Rastian Z*, et al.* (2018) Type I collagen from Jellyfish Catostylus mosaicus for biomaterial applications. *ACS Biomaterials Science & Engineering* 4(6):2115-2125.

14. Qureshi AH*, et al.* (2009) Proteomic and phospho-proteomic profile of human platelets in basal, resting state: insights into integrin signaling. *PLoS One* 4(10).

15. Chiu J (2019) Measurement of redox states of the β3 integrin disulfide bonds by mass spectrometry. *Bio-Protocol* 9:e3156.